A systematic evaluation of contemporary impurity correction methods in ITS-90 aluminium fixed point cells

Rodrigo da Silva[1,2], Jonathan V Pearce[1] and Graham Machin[1]

[1]National Physical Laboratory (NPL), Hampton Road, Teddington, Middlesex, TW11 0LW, United Kingdom
[2]Royal Holloway, University of London, Egham Hill, Egham, Surrey, TW20 0EX, United Kingdom

Email: rsilva.ufrj@gmail.com

Abstract

The fixed points of the International Temperature Scale of 1990 (ITS-90) are the basis of the calibration of standard platinum resistance thermometers (SPRTs). Impurities in the fixed point material at the level of parts per million can give rise to an elevation or depression of the fixed point temperature of order of millikelvins, which often represents the most significant contribution to the uncertainty of SPRT calibrations. A number of methods for correcting for the effect of impurities have been advocated, but it is becoming increasingly evident that no single method can be used in isolation. In this investigation, a suite of five aluminium fixed point cells (defined ITS-90 freezing temperature 660.323 °C) have been constructed, each cell using metal sourced from a different supplier. The five cells have very different levels and types of impurities. For each cell, chemical assays based on the glow discharge mass spectroscopy (GDMS) technique have been obtained from three separate laboratories. In addition a series of high quality, long duration freezing curves have been obtained for each cell, using three different high quality SPRTs, all measured under nominally identical conditions. The set of GDMS analyses and freezing curves were then used to compare the different proposed impurity correction methods. It was found that the most consistent corrections were obtained with a hybrid correction method based on the sum of individual estimates (SIE) and overall maximum estimate (OME), namely the SIE/Modified-OME method. Also highly consistent was the correction technique based on fitting a Scheil solidification model to the measured freezing curves, provided certain well defined constraints are applied. Importantly, the most consistent methods are those which do not depend significantly on the chemical assay.

Keywords: ITS-90, fixed point, aluminium, impurity, calibration, uncertainty, standard platinum resistance thermometer, traceability

1. Introduction

The International Temperature Scale of 1990 (ITS-90) [1] defines the phase transition temperature of a number of substances which are used as reference temperatures, or fixed points, for the calibration of standard platinum resistance thermometers (SPRTs) which are the interpolating instruments for the ITS-90. In many cases the largest contribution to the uncertainty of SPRT calibrations is the unknown elevation or depression of the freezing temperature due to the effect of trace impurities [2], which are typically present at levels of parts per million (ppm), even when metals of the highest purity are used in the construction of such fixed points [3].

Considerable work has been performed on the effect of impurities in ITS-90 fixed points, utilising various correction methods on individual cells (Sn [4, 5], Zn [6, 7, 8, 9], Al [10] and Ag [11]) and in fixed point cells in general [12, 13, 14, 15, 16]. Two key methods have emerged, and are now recommended by the CCT, which are both based on a chemical assay of the metal to determine which impurities are present, and in what quantity. These are the Sum of Individual Estimates (SIE) and Overall Maximum Estimate (OME) methods [2, 17]. The SIE method also requires a knowledge of the liquidus slope (rate of change of freezing temperature with impurity concentration) or distribution coefficient (molar ratio of solid solubility to liquid solubility of the impurity) in the low concentration limit, which

is often difficult to obtain, though substantial progress has been made in populating the record in the last few years [18].

A number of drawbacks of the SIE method have been pointed out [19, 20, 21, 22], in particular the high demand placed on the accuracy and sensitivity of chemical assays, and the unknown relationship between the sample analysed and the actual concentration of impurities in the fixed point cell after construction. A number of complementary methods have been proposed, which make use of the shape of the freezing curve itself [10, 22, 23, 24, 25, 26, 27, 28]. The principal advantage of these methods is the lack of dependence on chemical assays; however, this concern is replaced with the disadvantage that they rely heavily on various assumptions about the relationship between the shape of the freezing curve and the impurities. Ideally, an assessment of impurity effects would draw on a variety of different complementary techniques.

Among the ITS-90 metal fixed points, aluminium is of particular interest because of its importance in SPRT calibrations, being the highest temperature fixed point accessible to SPRTs, and a key fixed point for the calibration of high temperature SPRTs (HTSPRTs). It is also the most difficult to obtain in high purity so characterisation and quantification of impurity effects is crucial for this fixed point. It has also exhibited peculiar impurity effects [29, 30, 31, 32, 33, 34] including apparent significant oxidation [31]. Recently, after the publication of a comprehensive survey of distribution coefficients and liquidus slopes [35], it has become possible to fully implement the SIE for the aluminium point.

In this study, a suite of five aluminium fixed point cells have been constructed, each using metal from a different source. The aim was to have five cells exhibiting a wide range of impurity effects, so that the available impurity correction techniques can be applied to the five cells in a systematic way. The aim is to identify which techniques are most consistent across the five cells, and to examine any difficulties associated with the implementation of each method. The paper is laid out as follows. In Section 2 the construction of the fixed point cells is described. Section 3 describes the procedure for realising the freezes. The chemical analysis of the metals used in the cells is described in Section 4, and Section 5 provides an outline of the seven correction methods considered in this investigation. The results of the impurity corrections are given in Section 6, and these are discussed in Section 7. Finally, some conclusions are drawn.

2. Construction of the cells

2.1. Materials

To ensure a variation in the quantity and nature of impurities present in the aluminium used for construction of the suite of fixed point cells, a batch of aluminium was obtained from five different suppliers. Stated purity of each sample was of order 99.9999 % [by weight]. One supplier was from the UK, one from Japan, and three from the USA. Four of the samples were supplied in the form of shots/slugs, and one (from Japan) was supplied as a monolithic block, from which the required material was cut.

The graphite components, supplied by SGL Group, were stated by the manufacturer to be 99.9995 % pure and were supplied, in a cleaned state, from the manufacturer. The quartz tubes used for the cell envelope and re-entrant well were also supplied in a cleaned state by Cambridge Glassblowing Ltd. The argon gas (99.9999 % pure, contained in a dedicated cylinder) used for the atmosphere within the cell was supplied by Air Products. The graphite, the quartz tubes, and the gas were all sourced from companies NPL has been familiar with for many years.

2.2. Experimental details

The fixed point cells were constructed in accordance with the procedure outlined in [36]. The design has been tested and validated extensively, through good performance as demonstrated by international key comparisons [37, 38].

The design essentially consists of a high purity aluminium ingot contained within a graphite crucible. Above the crucible, there are graphite felt disks interspersed with graphite heat shunts. The system, which comprises an open fixed point cell design, is enclosed in a quartz tube, and also presents a quartz re-entrant well for the insertion of the temperature sensors. The system is sealed with a metal cap, which allows connection to an external gas handling system for pumping and backfilling with inert gas. A pressure gauge ensures operation at a pressure of 101,325 Pa (one atmosphere). The metal cap is cooled

by means of a continuously circulating water cooling arrangement. The open fixed point assembly is shown in figure 1.

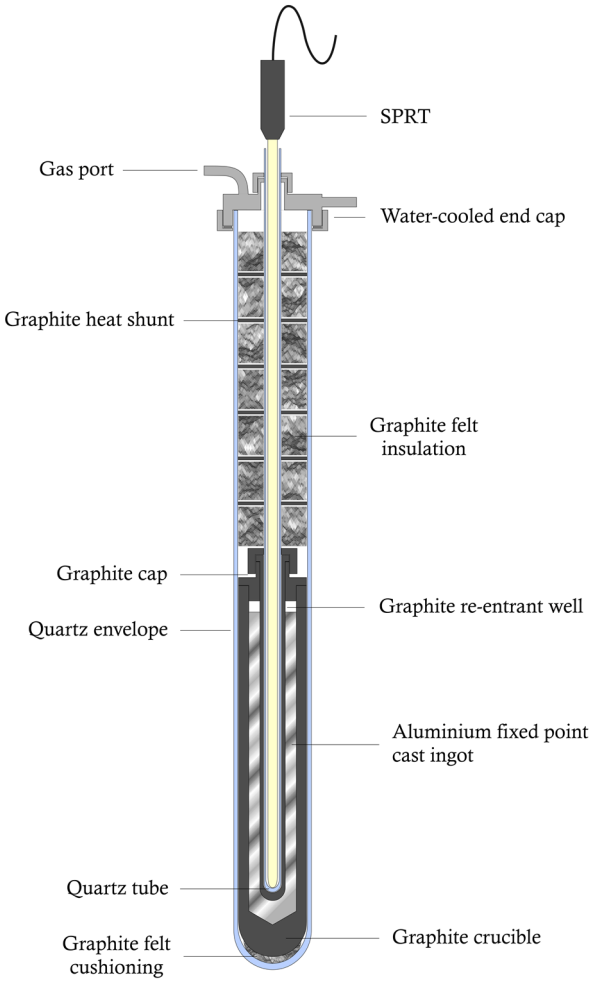

Figure 1. Design of the cell. The cell was installed in a commercial three-zone furnace which has been optimised to give extremely good temperature uniformity (gradient along the bottom-most 12 cm of the re-entrant well of the cell was less than 14 mK). A continuously circulating water cooling system was used to keep the top of the furnace, the cell cap and the SPRT head cool.

2.3. Casting

To avoid contamination the graphite components were kept in their original sealed packaging until the point of construction. Great care was taken to avoid contamination of all materials. The complete set of graphite parts for each cell were then baked inside a quartz tube in vacuum at a temperature of 1100 °C for approximately 48 hours. Each of the five sets of components was baked separately in the same dedicated quartz tube. The graphite felt disks were baked separately, in a different quartz tube, using a similar procedure.

In order to cast the aluminium ingots, each crucible was filled with sufficient aluminium to ensure a gap of about 10 mm between the surface of the metal and the inner surface of the graphite top cap. Once the metal was molten, the re-entrant tube was inserted. The casting was performed in a pure argon atmosphere at a pressure around 103 kPa (slightly overpressurisation) at a temperature of about 670 °C. After the ingot was cast, the cell was assembled. Selected stages are shown in figure 2 to illustrate the process.

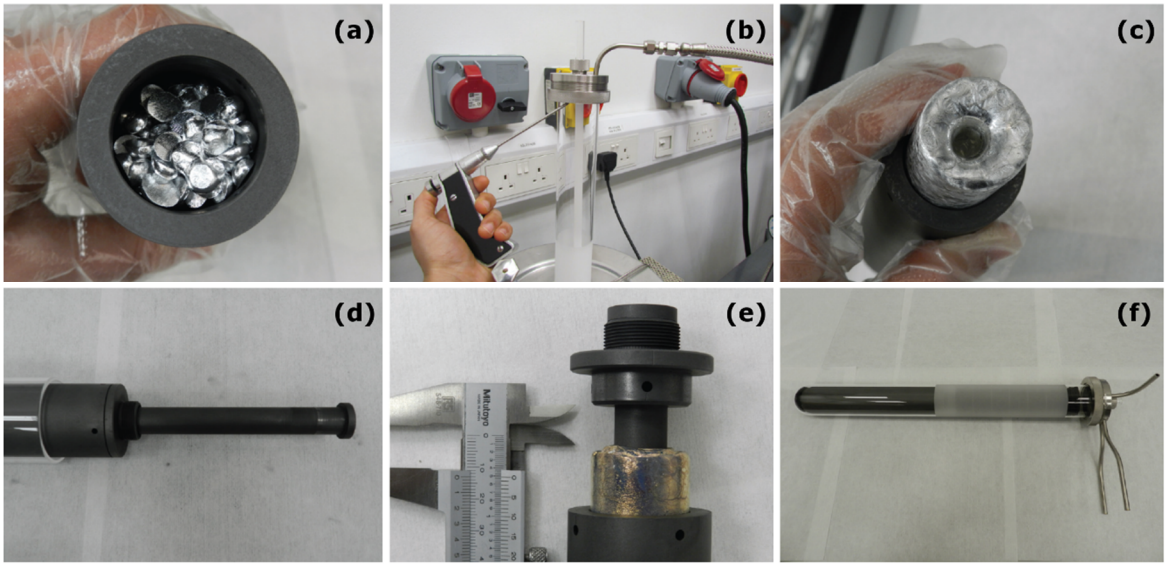

Figure 2. Selected stages of the construction process: (a) initial filling of the crucible with the aluminium; (b) leak testing the assembly containing the crucible before turning the furnace on; (c) inspection of the ingot cast after the initial filling; (d) reassembly of the crucible and insertion of the re-entrant well; (e) inspection of the completed ingot and (f) the cell fully assembled.

3. Realisation procedure

During the measurements, the pressure of argon gas inside the cell was maintained at 101,325 Pa. The temperature was measured using three 25.5 Ω SPRTs, each from a different manufacturer, and an ASL F900 resistance bridge. A 100 Ω standard resistor was maintained in a stirred oil bath at 20 °C which has a long term stability of about 0.004 °C. The output from the bridge was logged with dedicated data acquisition software. The SPRTs were annealed as per the generally accepted procedure [39] and calibrated by reference to NPL's national standard reference set of aluminium fixed points prior to use in the new cells.

Once set up in the furnace, each aluminium cell was continuously evacuated and heated until it reached approximately 655 °C (5 °C below the melting temperature). At this point it was slowly refilled with argon. This flushing was performed three times, before backfilling the cell with argon once more and adjusting the pressure to 101,325 Pa. The melt was then performed by increasing the furnace temperature to 5 °C above the aluminium melting temperature, and the pressure re-adjusted to 101,325 Pa. The cell was kept molten at this temperature for at least 20 hours, to facilitate mixing of the impurities by diffusion [27]. The freeze was initiated by cooling the furnace to 2.5 °C below the freezing temperature. On recalescence, a brass rod was inserted in the re-entrant well for one minute to create an inner solid-liquid interface. The freezing plateau was maintained by increasing the furnace temperature to 0.4 °C below the freezing point. This process yielded a typical freezing plateau duration of about 18 hours (10 mK range). Figure 3 shows typical freezing curves for the five cells measured with one SPRT. Each cell was used to realise freezing plateaus for about 4 weeks, amounting to at least 7 per cell. The repeatability of the freezing curve measurements is exemplified in Figure 4, where four curves measured consecutively with cell A are shown. The resistance of the three SPRTs was periodically measured at the triple point of water to check for drift.

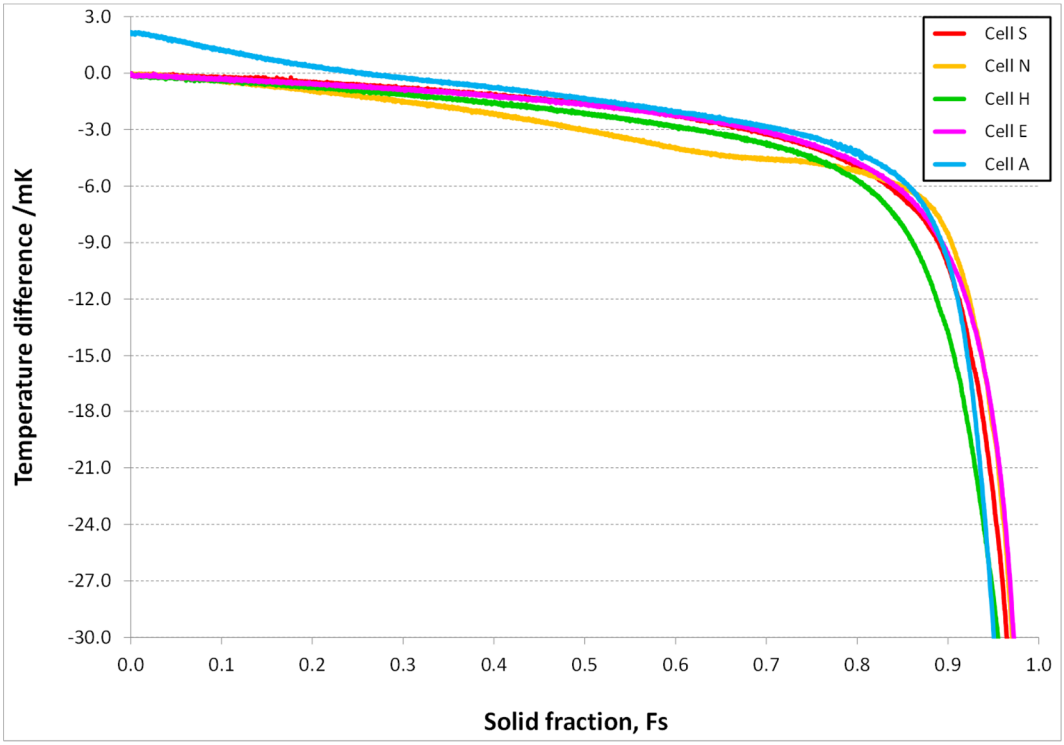

Figure 3. Typical curves from the five fixed point cells. For clarity, curves E, H, N, and S are shifted to ensure their maxima coincide. Cell A exhibits a steep descent at the start of the freeze, which is due to the influence of impurities having a high distribution coefficient. This curve was shifted up by 2.15 mK, for comparison purposes.

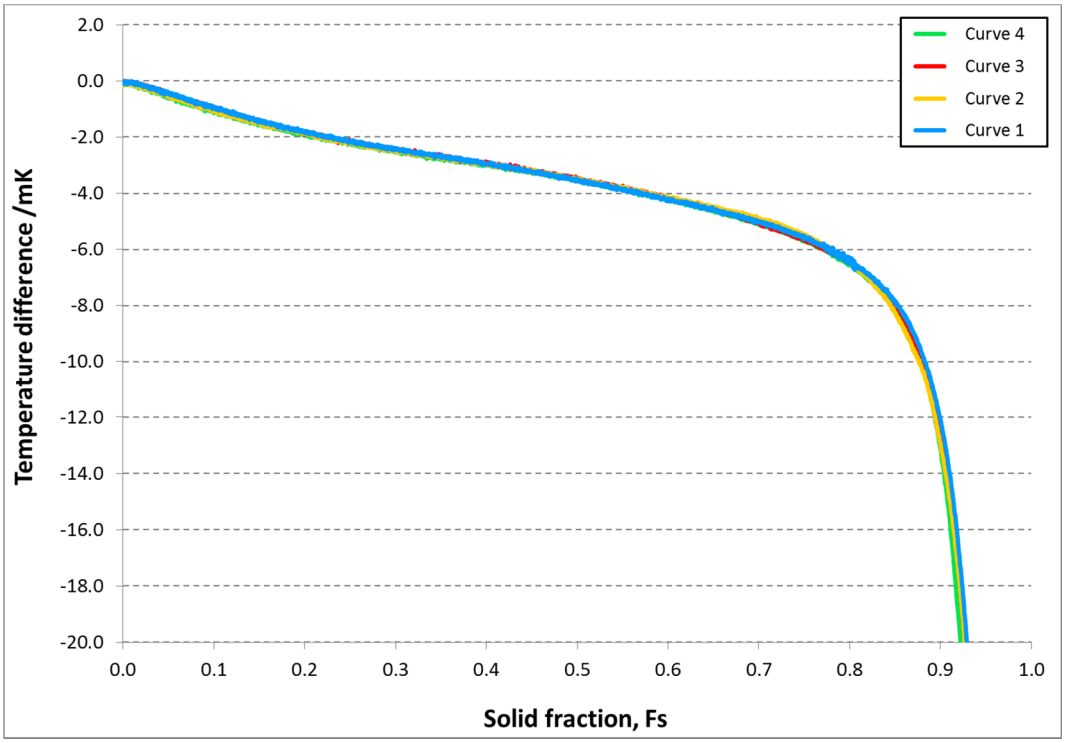

Figure 4. Four freezing curves measured for cell A with the same SPRT showing their repeatability.

4. Chemical analysis

To facilitate the implementation of the different correction methodologies, it is necessary to have a chemical analysis of the metal used for each cell. The most common method for analysing impurities in metals at the level of parts per million (ppm) is the glow discharge mass spectrometry (GDMS) technique. Some of the metals were provided with a chemical analysis; only three were performed with GDMS, the other two having been performed with inductively coupled plasma (ICP) spectrometry techniques. The ICP results revealed no impurities detected in one metal lot, and only 0.9 ppm of silicon in the other. In all cases, no information was provided on the uncertainty associated with the analysis.

Samples from each of the five metals were prepared and sent to three different laboratories to be analysed by GDMS. Each of these laboratories had a particular requirement for the sample shape and size to be sent to them. One required the sample to be in the shape of a flat cylinder (diameter 20 mm, height 5 mm) and the other required a thin pin (2.3 mm x 2.3 mm x 20 mm). The other was able to accept an assorted collection of randomly sized pellets. To produce the required geometries, graphite moulds were machined, cleaned, and baked at 900 °C so that the samples could be cast. Care was taken not to cross-contaminate the samples. The casting was performed under vacuum in a graphite furnace [40] at a temperature of about 700 °C. The system was held at this temperature for two hours, then cooled to room temperature at a rate of about 3 °C per minute. Figure 5 shows examples of the moulds and cast samples. On removal from the mould, the samples were cut to size as appropriate with a clean saw.

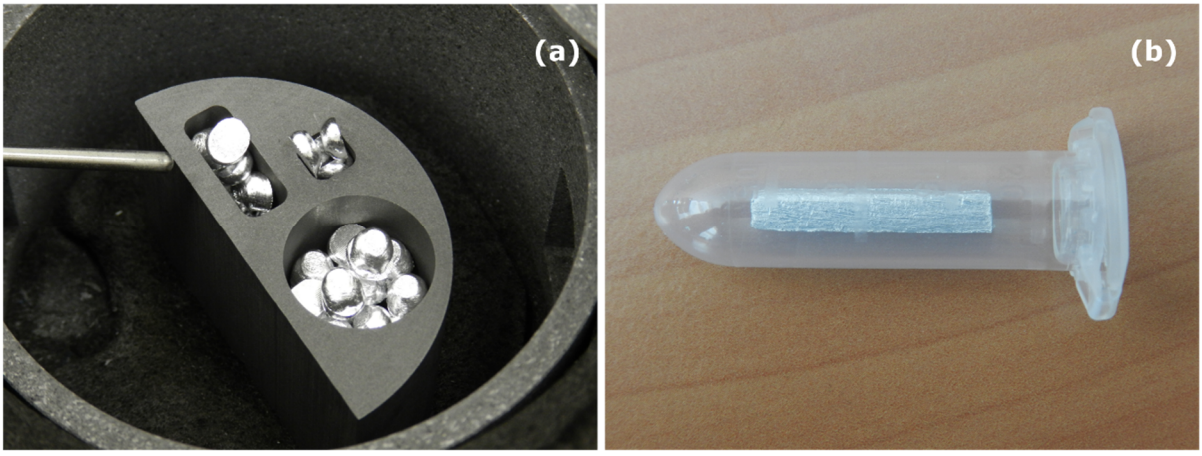

Figure 5. Sample preparation for the GDMS analysis: (a) samples (of the same lot) prior to melting and (b) long cylinder cut to size and ready for sending in its airtight container.

Scanning electron microscopy (SEM) and X-Ray photoelectron spectroscopy (XRS) analyses on the cut samples confirm that there was no significant contamination of the samples from the saw used to cut the pins. Figure 6 shows representative results from the SEM measurements.

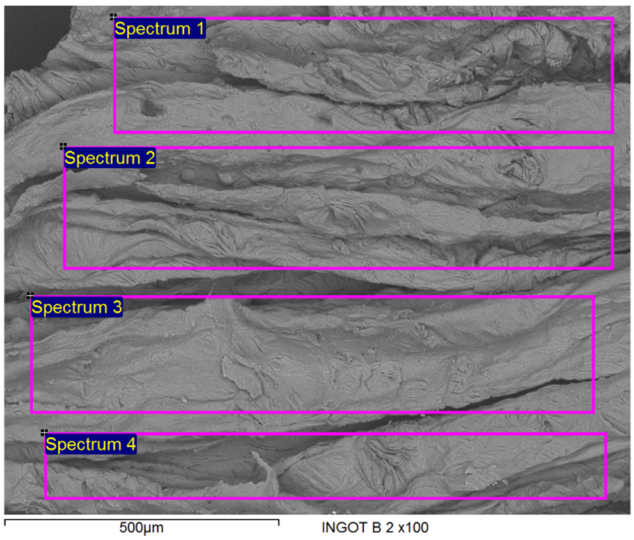

Spectrum	C	O	Al	Total
Spectrum 1	16.09	21.53	62.38	100.00
Spectrum 2	12.26	22.01	65.72	100.00
Spectrum 3	9.51	24.60	65.90	100.00
Spectrum 4	11.26	23.84	64.90	100.00
Mean	12.28	23.00	64.72	100.00
Std. deviation	2.78	1.46	1.63	
Max.	16.09	24.60	65.90	
Min.	9.51	21.53	62.38	

All results in weight %

Figure 6. The results of the SEM measurements showing principal constituents corresponding to the regions 1, 2, 3, and 4 on the image. No trace of Fe was observed which would have been expected if contamination had occurred from the cutting process.

The GDMS results for the aluminium from the five different suppliers (A, E, H, N, and S), are shown in tables 1-5. It is evident that for each sample there is little consistency between the GDMS analysis laboratories, which is a major limitation of impurity correction methodologies which rely on the GDMS analysis alone. Furthermore, none of the analyses carried a useable statement of uncertainty. GDMS suppliers 1 and 2 stated their uncertainties, although only as a percentage. Note that while the techniques making use of the chemical analyses assume the impurities are homogeneously distribute throughout the ingot, there may in fact be significant inhomogeneity [41]; here we assume the impurities are homogeneous.

Table 1. Results of the GDMS analyses for batch from metal supplier A.

Atomic No	Element	Impurity Concentration, ng/g			
		Supplier	Lab 1	Lab 2	Lab 3
1	H				
2	He				
3	Li	< 5	0.6	< 2	< 1
4	Be	< 5	< 6	< 0.9	< 1
5	B	< 5	20	12	11.30
6	C				
7	N				
8	O				
9	F	< 100		< 3	1230.75
10	Ne				
11	Na	< 5	40	< 1	268.50
12	Mg	78	100	30	10.55
13	Al	Matrix	Matrix	Matrix	
14	Si	186	400	780	2421.60
15	P	10	100	39	124.35
16	S	< 100	100	< 3	
17	Cl	< 100		5	3073.55
18	Ar				
19	K	< 100	90	< 4	40.45
20	Ca	< 20	100	< 20	83.25
21	Sc		40	64	61.30
22	Ti	37	600	640	479.15
23	V	24	20	28	21.30
24	Cr	35	40	69	111.95
25	Mn	34	40	47	25.35
26	Fe	14	200	830	99.25
27	Co	< 5	30	540	56.15
28	Ni	< 5	100	440	443.75
29	Cu	< 200	100	49	2946.45
30	Zn	< 50	50	26	321.80
31	Ga	< 5	7	< 5	8.15
32	Ge	< 40	< 20	< 9	1332.50
33	As	< 5	50	< 5	264.30
34	Se		≤ 40	< 30	112751.9
35	Br		≤ 40	< 11	833.00
36	Kr				
37	Rb		< 2	< 1	3.10
38	Sr		0.7	< 0.9	2.45
39	Y		< 0.7	< 0.8	1.50
40	Zr	< 5	4	280	7.65
41	Nb		3	13	15.60
42	Mo	< 2	10	< 5	104.35
43	Tc				
44	Ru		0.4		12.35
45	Rh		3		13.20
46	Pd	< 100	6		< 1
47	Ag	< 5	40	< 6	333.85

Atomic No	Element	Impurity Concentration, ng/g			
		Supplier	Lab 1	Lab 2	Lab 3
48	Cd	< 50	50	< 20	449.30
49	In	< 5	30	< 3	6.35
50	Sn	< 50	30	48	7.45
51	Sb	< 5	< 10	< 5	11.90
52	Te		10	26	36.35
53	I		≤ 2	< 2	1.40
54	Xe				
55	Cs	< 10	< 1	< 0.8	1.40
56	Ba	< 5	0.6	< 0.9	< 1
57	La	< 5	0.5	< 0.7	2.65
58	Ce	< 5	0.9	< 0.9	1.20
59	Pr		< 0.9		< 1
60	Nd	< 5	< 4		< 1
61	Pm				
62	Sm		5		< 1
63	Eu		< 2		3.45
64	Gd		< 3		12.75
65	Tb		< 1		1.15
66	Dy		< 4		< 1
67	Ho		< 0.9		2.25
68	Er		< 5		< 1
69	Tm		< 0.9		< 1
70	Yb		3		5.10
71	Lu		< 0.8		< 1
72	Hf		3	15	12.15
73	Ta				< 1
74	W	< 25	10	4	< 1
75	Re		6		3.55
76	Os		< 10		95.20
77	Ir		< 3		3.70
78	Pt	< 100	< 8	< 9	< 1
79	Au	< 10	2	< 1400	< 1
80	Hg	< 100	< 20	< 25	20.45
81	Tl		< 7	< 6	6.00
82	Pb	< 5	4	6	2488.25
83	Bi	< 5	6	< 3	6.45
84	Po				
85	At				
86	Rn				
87	Fr				
88	Ra				
89	Ac				
90	Th	< 700	< 0.1	< 0.9	1.30
91	Pa				
92	U	< 700	0.2	< 0.9	1.40
93	Np				
94	Pu				

Table 2. Results of the chemical analyses for batch from metal supplier E. The technique employed in the analysis provided by the supplier of the metal batch was ICP. No information was given about detection limits for the other elements scanned.

Atomic No	Element	Impurity Concentration, ng/g			
		Supplier	Lab 1	Lab 2	Lab 3
1	H				
2	He				
3	Li		< 0.3	< 3	< 1
4	Be		5	< 1	4.88
5	B		40	77	6.32
6	C				
7	N				
8	O				
9	F			< 2	185.32
10	Ne				
11	Na		20	< 1	27.05
12	Mg		300	73	35.95
13	Al	Matrix	Matrix	Matrix	
14	Si	900	800	920	813.50
15	P		50	18	13.25
16	S		100	< 4	
17	Cl			6	366.02
18	Ar				
19	K		30	< 4	8.95
20	Ca		< 30	< 20	23.58
21	Sc		30	69	60.40
22	Ti		30	71	85.70
23	V		30	49	62.60
24	Cr		50	57	66.70
25	Mn		50	33	38.15
26	Fe		200	220	54.58
27	Co		1	< 0.7	1.48
28	Ni		4	8	5.65
29	Cu		100	46	406.88
30	Zn		20	35	59.78
31	Ga		5	< 6	8.10
32	Ge		< 20	< 10	253.90
33	As		40	< 6	70.50
34	Se		≤ 40	< 40	13306.42
35	Br		≤ 40	< 12	108.82
36	Kr				
37	Rb		< 2	< 2	0.52
38	Sr		< 0.9	< 0.9	0.82
39	Y		< 0.8	< 1	0.40
40	Zr		7	180	15.75
41	Nb		< 0.9	4	0.62
42	Mo		10	< 2	27.08
43	Tc				
44	Ru		1		12.72
45	Rh		2		2.92
46	Pd		< 10		16.50
47	Ag		10	< 7	84.12

Atomic No	Element	Impurity Concentration, ng/g			
		Supplier	Lab 1	Lab 2	Lab 3
48	Cd		30	27	53.00
49	In		20	41	0.60
50	Sn		70	< 43	4.05
51	Sb		20	< 9	3.35
52	Te		< 20	18	8.20
53	I		≤ 1	< 3	0.38
54	Xe				
55	Cs		< 1	< 1	0.80
56	Ba		< 1	< 1	< 1
57	La		8	9	0.50
58	Ce		10	20	0.18
59	Pr		1		0.30
60	Nd		10		2.98
61	Pm				
62	Sm		< 4		6.20
63	Eu		< 2		1.00
64	Gd		< 4		0.92
65	Tb		< 1		< 1
66	Dy		< 5		1.65
67	Ho		< 1		0.65
68	Er		< 3		1.30
69	Tm		< 1		0.45
70	Yb		< 4		0.78
71	Lu		< 1		0.15
72	Hf		0.3	< 4	2.78
73	Ta				0.95
74	W		20	< 3	1.20
75	Re		7		1.02
76	Os		< 20		4.38
77	Ir		< 3		0.70
78	Pt		< 10	< 11	5.90
79	Au		4	< 920	1.88
80	Hg		< 20	< 32	11.32
81	Tl		< 8	< 8	4.65
82	Pb		10	8	129.15
83	Bi		1700	21	0.92
84	Po				
85	At				
86	Rn				
87	Fr				
88	Ra				
89	Ac				
90	Th		0.5	< 1	0.38
91	Pa				
92	U		0.1	< 1	0.20
93	Np				
94	Pu				

Table 3. Results of the chemical analyses for batch from metal supplier H. The technique employed in the analysis provided by the supplier of the metal batch was ICP-AES. As it detected no impurities, calculations were based on half of the detection limits stated for the scanned elements, following CCT recommendations [17, 42]. However this seems to yield a significant overestimation of the real impurity levels in the material.

Atomic No	Element	Impurity Concentration, ng/g			
		Supplier	Lab 1	Lab 2	Lab 3
1	H				
2	He				
3	Li		0.5	< 2	13.10
4	Be	< 100	5	< 0.9	1.25
5	B	< 100	9	22	11.88
6	C				
7	N				
8	O				
9	F			< 2	428.50
10	Ne				
11	Na		20	< 1	60.05
12	Mg	< 100	200	270	135.73
13	Al	Matrix	Matrix	Matrix	
14	Si	< 500	400	500	1116.85
15	P	< 5000	30	7	54.03
16	S		50	< 3	
17	Cl			7	927.68
18	Ar				
19	K		30	< 4	16.93
20	Ca	< 500	< 30	< 17	56.20
21	Sc		30	53	34.03
22	Ti	< 100	50	52	95.13
23	V	< 100	20	29	30.18
24	Cr	< 100	20	25	17.45
25	Mn	< 100	20	14	20.78
26	Fe	< 100	100	220	130.17
27	Co	< 100	< 2	< 0.4	4.25
28	Ni	< 300	5	4	5.65
29	Cu	< 100	70	23	781.70
30	Zn	< 500	40	24	40.20
31	Ga	< 100	5	< 5	4.43
32	Ge	< 1000	< 20	< 8	394.13
33	As	< 2000	40	< 5	96.18
34	Se		< 60	< 70	19056.03
35	Br		≤ 30	< 10	122.03
36	Kr				
37	Rb		< 2	< 1	0.85
38	Sr	< 100	< 0.9	< 0.6	0.30
39	Y		< 0.8	< 0.8	0.13
40	Zr	< 100	20	130	23.93
41	Nb		< 0.9	3	0.45
42	Mo	< 500	6	< 2	32.73
43	Tc				
44	Ru		0.5		3.40
45	Rh		2		1.60
46	Pd	< 200	< 9		7.95
47	Ag	< 100	10	< 6	89.05
48	Cd	< 100	80	26	70.43
49	In	< 500	10	15	0.35
50	Sn	< 1000	300	290	2.58
51	Sb	< 1000	< 10	< 7	6.40
52	Te	< 5000	< 20	21	51.98
53	I		< 1	< 2	< 1
54	Xe				
55	Cs		< 1	< 0.8	0.98
56	Ba	< 100	< 1	< 0.9	5.88
57	La		< 0.9	< 0.6	< 1
58	Ce		< 1	< 0.6	9.13
59	Pr		< 1		1.00
60	Nd		< 5		< 1
61	Pm				
62	Sm		< 4		3.93
63	Eu		< 2		0.95
64	Gd		< 4		1.15
65	Tb		< 1		0.60
66	Dy		< 4		3.13
67	Ho		< 1		< 1
68	Er		< 3		0.80
69	Tm		< 1		0.38
70	Yb		< 4		2.70
71	Lu		< 1		0.33
72	Hf		1	< 3	31.18
73	Ta				0.93
74	W		10	< 2	61.40
75	Re		< 2		< 1
76	Os		< 20		7.67
77	Ir		3		1.28
78	Pt	< 1000	< 10	< 8	1.73
79	Au	< 100	3	< 1300	0.58
80	Hg	< 500	< 20	< 25	5.00
81	Tl	< 1000	< 8	< 6	1.73
82	Pb	< 2000	4	8	114.43
83	Bi	< 3000	20	< 3	1.68
84	Po	< 100			
85	At	< 500			
86	Rn	< 1000			
87	Fr	< 1000			
88	Ra	< 5000			
89	Ac				
90	Th		0.1	< 0.8	0.93
91	Pa				
92	U	< 100	0.1	< 0.8	0.48
93	Np				
94	Pu				

Table 4. Results of the GDMS analyses for batch from metal supplier N.

Atomic No	Element	Impurity Concentration, ng/g			
		Supplier	Lab 1	Lab 2	Lab 3
1	H				
2	He				
3	Li	< 5	0.4	< 3	17.90
4	Be	< 5	< 8	< 1	2.17
5	B	< 5	10	< 2	6.97
6	C				
7	N				
8	O				
9	F			< 4	301.07
10	Ne				
11	Na	< 5	20	< 1	170.60
12	Mg	88	100	37	3.67
13	Al	Matrix	Matrix	Matrix	
14	Si	154	200	180	562.13
15	P		30	< 3	15.80
16	S		50	< 4	
17	Cl			< 2	528.20
18	Ar				
19	K	< 100	10	< 4	9.30
20	Ca	< 20	50	< 16	48.57
21	Sc		40	52	54.33
22	Ti	58	30	49	44.73
23	V	17	10	23	22.97
24	Cr	37	40	40	65.00
25	Mn	24	30	37	50.63
26	Fe	7	100	260	34.90
27	Co	< 5	< 2	< 0.6	1.33
28	Ni	< 5	5	< 2	19.93
29	Cu	< 200	30	25	494.43
30	Zn	< 50	30	23	52.03
31	Ga	< 5	4	< 5	< 0.01
32	Ge	< 40	< 30	< 9	386.13
33	As	< 5	30	< 3	86.40
34	Se		50	< 70	33655.10
35	Br		≤ 30	< 10	258.57
36	Kr				
37	Rb		< 2	< 1	1.67
38	Sr		< 1	< 0.8	0.10
39	Y		< 0.8	< 0.9	0.23
40	Zr	< 5	1	110	2.83
41	Nb		< 1	5	0.30
42	Mo	< 5	9	< 2	5.00
43	Tc				
44	Ru		0.4		5.80
45	Rh		2		1.77
46	Pd	< 100	10		13.97
47	Ag	< 5	6	< 7	124.40

Atomic No	Element	Impurity Concentration, ng/g			
		Supplier	Lab 1	Lab 2	Lab 3
48	Cd	< 50	30	< 22	958.27
49	In	< 5	9	< 2	0.67
50	Sn	< 50	40	150	2.30
51	Sb	< 5	10	< 5	< 0.01
52	Te		< 20	23	13.57
53	I		< 2	< 3	1.30
54	Xe				
55	Cs	< 10	< 2	< 0.9	0.43
56	Ba	< 5	< 1	< 1	4.30
57	La	< 5	1	< 0.7	0.53
58	Ce	< 5	< 1	< 0.7	0.73
59	Pr		< 1		0.33
60	Nd	< 5000	< 6		< 0.01
61	Pm				
62	Sm		< 4		< 0.01
63	Eu		< 2		< 0.01
64	Gd		< 4		3.97
65	Tb		< 1		0.73
66	Dy		< 5		1.80
67	Ho		< 1		0.70
68	Er		< 4		1.43
69	Tm		< 1		0.67
70	Yb		< 4		1.57
71	Lu		< 1		0.60
72	Hf		0.7	< 4	1.27
73	Ta				< 0.01
74	W	< 25	9	5	< 0.01
75	Re		10		1.10
76	Os		< 20		< 0.01
77	Ir		< 3		0.73
78	Pt	< 100	20	< 8	3.10
79	Au	< 10	3	< 1300	2.07
80	Hg	< 50	< 20	< 29	< 0.01
81	Tl		< 9	< 7	4.03
82	Pb	< 5	< 3	< 3	440.40
83	Bi	< 5	6	< 3	2.03
84	Po				
85	At				
86	Rn				
87	Fr				
88	Ra				
89	Ac				
90	Th	< 0.7	0.1	< 0.8	0.40
91	Pa				
92	U	< 0.7	< 0.1	< 1	< 0.01
93	Np				
94	Pu				

Table 5. Results of the GDMS analyses for batch from metal supplier S.

Atomic No	Element	Impurity Concentration, ng/g			
		Supplier	Lab 1	Lab 2	Lab 3
1	H				
2	He				
3	Li	< 1	< 1	< 2	71.75
4	Be	< 1	7	< 0.8	1.75
5	B	< 10	60	< 1	125.80
6	C				
7	N				
8	O				
9	F			< 3	374.45
10	Ne				
11	Na	4	30	< 1	118.98
12	Mg	45	50	76	2.43
13	Al	Matrix	Matrix	Matrix	Matrix
14	Si	270	400	330	735.05
15	P		30	12	11.65
16	S		100	< 3	
17	Cl			9	1204.83
18	Ar				
19	K	< 100	20	< 4	21.10
20	Ca	< 50	90	< 16	20.90
21	Sc		40	57	34.45
22	Ti	10	40	10	19.65
23	V	65	40	61	58.93
24	Cr	15	40	15	32.45
25	Mn	3	10	4	10.25
26	Fe	55	200	70	98.70
27	Co	< 1	2	< 0.5	0.38
28	Ni	10	20	9	8.03
29	Cu	57	400	18	516.87
30	Zn	< 2	20	27	141.53
31	Ga	< 1	10	< 4	12.20
32	Ge	< 50	< 30	< 7	467.50
33	As	< 5	50	< 4	137.00
34	Se	< 30	70	< 60	25090.53
35	Br	< 50	≤ 30	< 10	193.90
36	Kr				
37	Rb		2	< 1	1.73
38	Sr		< 1	< 0.6	3.48
39	Y		< 0.8	< 0.7	0.58
40	Zr	7	5	62	3.83
41	Nb	3	0.7	2	0.93
42	Mo	24	40	< 2	32.13
43	Tc				
44	Ru		0.7		7.83
45	Rh		2		0.95
46	Pd		< 10		103.48
47	Ag	< 1	10	< 6	891.08
48	Cd	< 10	50	89	55.80
49	In	< 1	8	74	< 1
50	Sn	< 20	300	< 32	1.83
51	Sb	< 5	< 10	< 9	14.83
52	Te		10	22	7.30
53	I		< 2	< 2	1.05
54	Xe				
55	Cs	< 1	< 2	< 0.6	0.38
56	Ba	< 1	1	< 0.7	6.90
57	La	< 1	< 1	< 0.6	0.68
58	Ce	< 1	< 1	< 0.6	0.60
59	Pr		< 1		1.10
60	Nd	< 3	< 6		3.58
61	Pm				
62	Sm		< 4		3.78
63	Eu		< 2		0.43
64	Gd		< 5		4.80
65	Tb		< 1		0.85
66	Dy		< 5		2.85
67	Ho		< 1		0.28
68	Er		< 4		1.15
69	Tm		< 1		1.05
70	Yb		< 4		1.28
71	Lu		< 1		0.25
72	Hf	< 1	7	< 3	< 1
73	Ta				0.43
74	W	< 1	70	< 2	2.13
75	Re		< 2		0.90
76	Os		< 20		< 1
77	Ir		< 4		1.20
78	Pt	< 2	< 10	< 8	7.48
79	Au		5	< 1100	0.83
80	Hg	< 10	< 20	< 24	5.08
81	Tl	< 1	< 9	< 6	4.83
82	Pb	< 1	5	8	173.85
83	Bi	< 1	30	< 3	2.08
84	Po				
85	At				
86	Rn				
87	Fr				
88	Ra				
89	Ac				
90	Th	< 0.3	< 0.1	< 0.6	1.90
91	Pa				
92	U	< 0.3	0.1	< 0.8	0.73
93	Np				
94	Pu				

5. Current methodologies for estimating the effect of impurities in fixed point cells

Impurity effects often represent the largest contribution to the uncertainty associated with the realisation of an ITS-90 metal fixed-point [2]. The effect is often so large that it is desirable to perform some correction to account for it. The CCT has provided a recommendation [17] on how to approach this correction but this has serious shortcomings and a number of other techniques have been proposed and discussed. The available methods can be divided into two categories: those that depend on chemical analysis, and those that depend on analysis of the shape of the freezing curve. There are several methods that depend on both. The principal correction methods that depend on chemical analysis are the Sum of Individual Estimates (SIE); the Overall Maximum Estimate (OME); the Hybrid SIE/OME. Those that depend on the shape of the freezing curve are; the Scheil model; the gradient method; the thermal analysis, or '1/F method'; and the direct comparison of cells. In this section, these are summarised in the context of the current investigation.

5.1 Sum of Individual Estimates (SIE)

The SIE method relies on the assumption that the effect of each impurity in the metal is independent of the others [43] so that the effect of all the impurities on the freezing temperature can be summed over

all impurities. It is currently the method recommended by the CCT [17]. It also relies on a knowledge of the amount of each impurity present, provided by the GDMS analysis, and the liquidus slope in the limit of low concentration. The change in the freezing temperature caused by the impurities is given by

$$\Delta T_{\mathrm{SIE}} = T_{\mathrm{pure}} - T_{\mathrm{liq}} = -\sum_i c_i \cdot m_i \tag{1}$$

where T_{pure} is the freezing temperature of the ideally pure material and T_{liq} is the actual freezing temperature. Both T_{pure} and T_{liq} represent the liquidus point. c_i is the concentration of impurity i and m_i is its liquidus slope. The values of the distribution coefficient (k) and liquidus slopes used in this investigation are given as a function of atomic number Z up to Z = 94 in table 6 [18, 35]. The uncertainty in the value of ΔT_{SIE} is:

$$u^2(\Delta T_{SIE}) = \sum_i [u(c_i) \cdot m_i]^2 + [c_i \cdot u(m_i)]^2 \tag{2}$$

Table 6. Values of the distribution coefficient k and liquidus slopes of impurities in aluminium in the low concentration limit [18, 35].

Atomic No	Element	k	m^i_l µK/ppbw
1	H	0.020	-17.873
2	He	0.000	-4.527
3	Li	0.961	-1.319
4	Be	0.177	-1.832
5	B	0.099	-1.858
6	C	0.001	-1.131
7	N	0.019	-1.276
8	O	0.654	-0.396
9	F	0.000	0.000
10	Ne	0.000	-0.898
11	Na	0.010	-0.724
12	Mg	0.356	-0.450
13	Al	1.000	0.000
14	Si	0.089	-0.623
15	P	0.011	-0.834
16	S	0.002	-0.511
17	Cl	0.000	0.000
18	Ar	0.000	-0.453
19	K	0.280	-0.277
20	Ca	0.031	-0.470
21	Sc	0.479	-0.223
22	Ti	6.741	4.607
23	V	4.940	3.321
24	Cr	1.968	1.051
25	Mn	0.743	0.115
26	Fe	0.183	-0.311
27	Co	0.016	-0.297
28	Ni	0.195	-0.309
29	Cu	0.367	-0.252
30	Zn	0.512	-0.037
31	Ga	0.146	-0.150
32	Ge	0.055	-0.208
33	As	0.009	-0.235
34	Se	0.003	-0.288
35	Br	0.000	-0.227
36	Kr	0.000	-0.216
37	Rb	0.003	-0.160
38	Sr	0.026	-0.196
39	Y	0.019	-0.192
40	Zr	2.406	1.233
41	Nb	2.963	5.478
42	Mo	2.117	1.155
43	Tc	0.100	0.045
44	Ru	0.077	-0.143
45	Rh	0.053	0.068
46	Pd	0.044	-0.057
47	Ag	0.435	0.010
48	Cd	0.287	-0.112
49	In	0.139	-0.157
50	Sn	0.020	-0.142
51	Sb	0.267	-0.081
52	Te	0.035	-0.116
53	I	0.020	0.000
54	Xe	0.001	-0.137
55	Cs	0.003	-0.104
56	Ba	0.003	-0.079
57	La	0.010	-0.121
58	Ce	0.002	-0.128
59	Pr	0.002	-0.127
60	Nd	0.001	-0.125
61	Pm	0.000	0.000
62	Sm	0.020	-0.110
63	Eu	0.000	-0.119
64	Gd	0.010	-0.115
65	Tb	0.017	-0.107
66	Dy	0.020	-0.101
67	Ho	0.020	-0.099
68	Er	0.020	-0.098
69	Tm	0.008	-0.104
70	Yb	0.040	-0.046
71	Lu	0.000	-0.104
72	Hf	4.087	2.391
73	Ta	8.555	5.443
74	W	2.557	0.488
75	Re	1.000	0.095
76	Os	0.031	0.400
77	Ir	0.030	0.376
78	Pt	0.310	0.017
79	Au	0.109	-0.010
80	Hg	0.130	-0.030
81	Tl	0.020	-0.059
82	Pb	0.093	-0.052
83	Bi	0.082	-0.039
84	Po	0.000	0.000
85	At	0.000	0.000
86	Rn	0.000	-0.081
87	Fr	0.000	0.000
88	Ra	0.000	0.000
89	Ac	0.000	0.000
90	Th	0.053	-0.052
91	Pa	0.020	-0.079
92	U	0.004	-0.060
93	Np	0.020	-0.077
94	Pu	0.004	-0.049

5.2 Overall Maximum Estimate (OME)

Whenever there is not sufficient knowledge of the impurity concentrations or their liquidus slopes, the CCT recommends the use of the OME method [17], which only requires a knowledge of the overall mole fraction impurity concentration and the first cryoscopic constant [44] for the fixed point material. This method does not provide a correction to the freezing temperature; instead, it yields a value which can be used to represent the uncertainty in the temperature:

$$\Delta T_{\mathrm{OME}} = \frac{c}{A} \tag{3}$$

Where c is the overall impurity concentration, and A is the cryoscopic constant, which is given by

$$A = \frac{L}{R[T_{pure}]^2} \tag{4}$$

Where L is the molar heat of fusion, R is the molar gas constant, and T_{pure} is the phase transition temperature of the pure substance.

The uncertainty in ΔT_{OME} is given by

$$u^2(\Delta T_{\mathrm{OME}}) = \frac{\left[\frac{c}{A}\right]^2}{3} \tag{5}$$

As the GDMS analyses in this study are rather complete, and the published list of common impurities is well represented in the analyses [42], the overall concentration of impurities can be estimated from the GDMS analyses themselves.

5.3 Hybrid SIE/Modified-OME

This method combines the SIE method for the dominant impurities and the OME method for the remaining impurities [17]. If the equilibrium distribution coefficients k of all relevant impurities are known, which is now the case for aluminium [18, 35], a simpler, modified OME method can be used. The change in the liquidus-point temperature by impurities with k less than 0.1, can be reliably estimated by fitting the expression

$$T_{pure} - T_{liq,\leq 0.1} = \frac{c}{FA} \tag{6}$$

to the freezing curve over an appropriate range (typically within the first half of the freeze). F is the liquid fraction. It is acceptable to determine the concentration of impurities with $k > 0.1$ by parameterisation using a least-squares fit of (6) to the measured freezing curve, then apply (3) to determine ΔT_{OME}. For the remaining impurities, $k \geq 0.1$, the SIE method is applied to those impurities having $k \geq 0.1$ to determine ΔT_{SIE}. The two estimates are then summed.

In this investigation, the OME component was estimated by fitting data at the beginning of the freezing curve ($0.05 < 1 - F < 0.15$) using (6). To perform the fitting, it is necessary for the freezing curve abscissa to be in terms of solid fraction $1 - F$, and the ordinate to be in terms of temperature. The peak in the freezing plateau is defined as occurring at $1 - F = 0$, and ΔT is specified as zero at this point. To convert the elapsed time to solid fraction, it is necessary to define an end point. This is taken to be the point of inflection in the curve after the steep drop in temperature following the end of the flat part of the curve, prior to the approach to the furnace temperature; this has been found to coincide with the disappearance of the liquid-solid interface determined with more rigorous methods [25].

The uncertainty in this hybrid method may be determined by combining the uncertainty of the two individual corrections in quadrature.

5.4 Scheil model

The Scheil model of solidification makes the assumption that diffusion processes are very fast compared with the velocity of the liquid-solid interface [25, 27]. In practical terms, this means freezing durations of greater than about 12 hours. The temperature is related to the liquid fraction F by

$$T = T_0 + mcF^{k-1} \tag{7}$$

where c is the overall concentration of impurities, m is the liquidus slope, and k is the distribution coefficient. By fitting this expression to the freezing curve using least-squares methods, the quantity mc can be obtained, which is the change in temperature due to the impurities corresponding to $F = 1$. Note that m and c cannot be parameterised independently because of their linear interdependence during the fitting process.

The main drawback of this method is the degeneracy associated with the existence of several impurities having different values of k. In this case, different combinations of impurities can all give rise to the same value of mc, which means that in some cases the model is not able to uniquely identify the temperature correction. Nonetheless, this method provides useful additional information on the impurity effects, and, importantly, does not rely on the GDMS analysis. In this study, the uncertainty attributed to the correction yielded by the Scheil method was obtained from the uncertainty in the value of the fitted parameter mc arising from the least-squares fit. Care should be taken to perform the fitting only in the region of the freezing curve where the shape is dominated by impurity effects, i.e. towards the early parts of the freeze. Towards the end of the freeze, the shape gradually becomes dominated by thermal effects as the liquid-solid interface reaches the re-entrant well and the corresponding immersion of the SPRT sensing element deteriorates. Figure 7 shows a typical fit of the Scheil model.

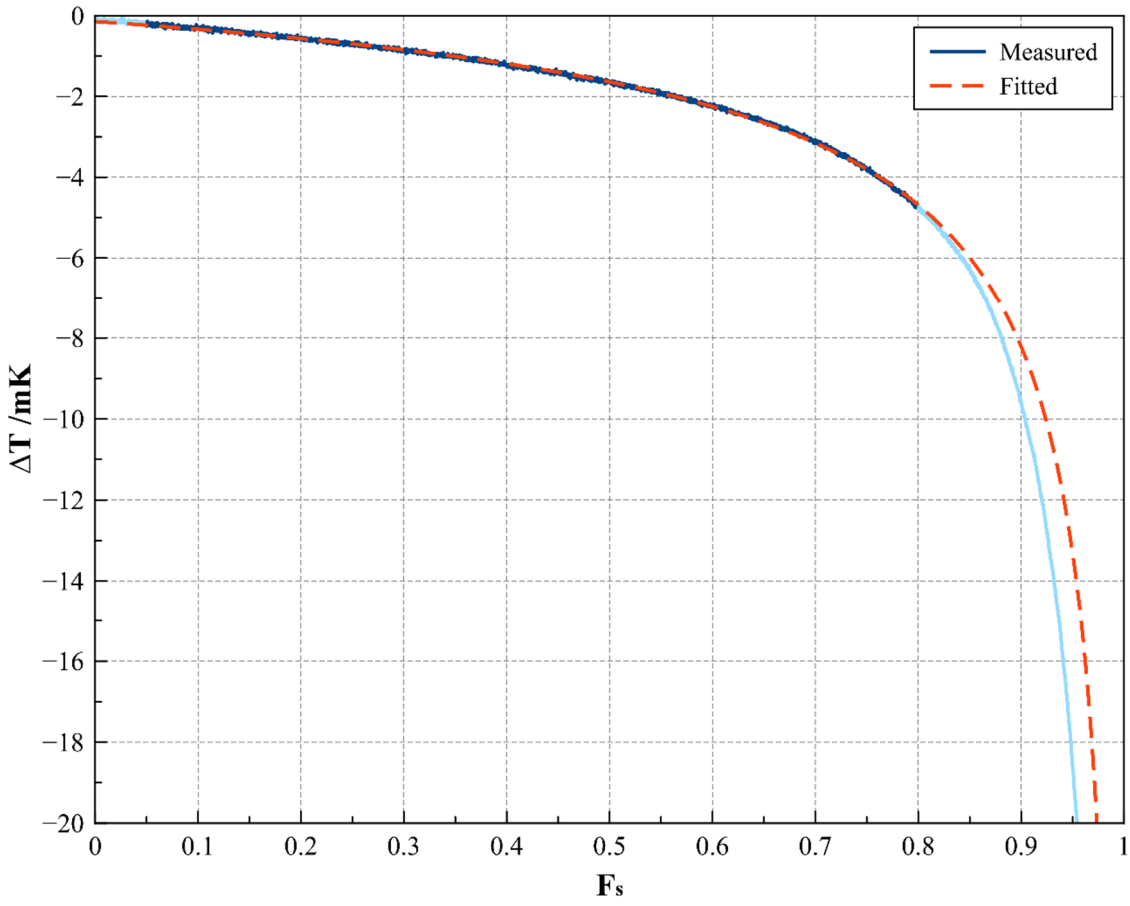

Figure 7. Fit of the Scheil expression (6) to experimentally measured freezing curve. T_0, mc, and k are free parameters.

5.5 Gradient method

The gradient method is derived from the Scheil method [26]. It is a fast way of estimating the impurity correction. The gradient of the freezing curve at $F = 0.5$ is determined by fitting a tangent to the freezing curve at that point (over the range $0.45 < F < 0.55$), and extrapolating it to $F = 0$. The estimate is given by

$$T_0 = T_T + \frac{T_T - T_{F=1}}{(1-k)} \tag{8}$$

Where T_T is the temperature at $F = 0.5$. The method is only applicable for systems where $k = 0$. The uncertainty in the correction is taken to be the uncertainty associated with the fitting process.

5.6 Thermal analysis

The '1/*F* method', sometimes called 'thermal analysis' is a variation of the Scheil method, with *k* assumed to be zero [10, 22, 23]. In this case, the temperature is plotted as a function of 1/*F*, which allows a straight line to be fitted to the linear portion of the data in the early part of the freeze, where the shape of the freezing curve is dominated by impurity effects. The gradient of this line can then be used to yield a parameter $dT / d(1/F)_{1/F=1}$ [10], which is taken to represent the correction at $F = 1$. The uncertainty associated with the correction was obtained from the uncertainty in the value of the fitted gradient arising from the least-squares fit.

5.7 Direct cell comparison

The direct comparison of freezing curves is a widely used *de-facto* standard method of comparing the freezing temperatures. This method cannot be used to determine absolute corrections for impurity effects, but can be used to examine relative differences between cells. To achieve the most reliable results it is essential that the SPRT used for the comparison is stable, and that the thermal environment of the cells is essentially the same. In this investigation the same furnace was used for all five cells constructed, which were compared against the NPL national reference standard cell. The SPRT was carefully quenched and measured at the triple point of water between measurements to express the comparison in terms of the ratio of the resistance at the aluminium freezing temperature and the resistance at the triple point of water, namely *W*. In addition, all measurements were corrected for self-heating, hydrostatic head, and pressure differences. As with all measurements performed in this investigation, the cell was held in the molten state for 20 hours prior to beginning the freeze. The uncertainty budget for the comparison measurements is shown in table 7.

Table 7. Uncertainty budget for the direct comparison of cells. It is worth observing that the major component in this approach is the uncertainty of the traceable reference cell, which in turn was compared to the national standard previously (when this component becomes the effect of impurities).

Uncertainty at the Freezing Point of Aluminium

Component	Description	Standard Uncertainty	Sensitivity Coefficient	Uncertainty Contribution /mK
Al - A1	Repeatability of readings (0 mA)	0.4 E-7 Ω/Ω	1250 K	0.080
Al - B1	Uncertainty of traceable reference cell	0.858 mK	1	0.858
Al - B2	Hydrostatic pressure correction	10 mm (÷ √3)	1.6 mK/m	0.009
Al - B3	Argon pressure in cell	2.6 kPa (÷ √3)	7.0 E-8 K/Pa	0.106
Al - B4	Perturbing heat exchanges	0.7 mK (÷ √3)	1	0.214
Al - B5	Self-heating extrapolation: bridge current ratio	2% of SHE (3 mK)	1	0.035
Al - B6	Bridge linearity	0.5 E-7 Ω/Ω (÷ √3)	1250 K	0.036
Al - B7	Temperature of Rs	20 mK (÷ √3)	1.05 mK/ppm	0.022
Al - B8	AC/DC, frequency, etc	0.7E-7 Ω/Ω (÷ √3)	1250 K	0.051
	Sub-total at FP Al			**0.897**

Uncertainty at the Triple Point of Water

Component	Description	Standard Uncertainty	Sensitivity Coefficient	Uncertainty Contribution /mK
TPW - A1	Repeatability of readings (0 mA)	0.05 E-7 Ω/Ω	1000 K	0.008
TPW - B1	Uncertainty of TPW cell	0.034 mK	1	0.034
TPW - B2	Hydrostatic pressure correction	5 mm (÷ √3)	0.73 mK/m	0.002
TPW - B3	Perturbing heat exchanges	0.01 mK (÷ √3)	1	0.006
TPW - B4	Self-heating extrapolation: bridge current ratio	2% of SHE (3 mK)	1	0.035
TPW - B5	Bridge linearity	0.5 E-7 Ω/Ω (÷ √3)	1000 K	0.029
TPW - B6	Temperature of Rs	20 mK (÷ √3)	0.25 mK/ppm	0.005
TPW - B7	AC/DC, frequency, etc	0.27E-7 Ω/Ω (÷ √3)	1000 K	0.016
	Sub-total at TPW			**0.059**
	Equivalent at FP Al	0.059 mK	4.2	**0.250**
		Combined uncertainty (*k* = 1)		**0.931**

6. Results

The results obtained from the methodologies of Section 5 are outlined below. The results are grouped by cell (i.e. metal supplier). All uncertainties correspond to a coverage factor of $k = 1$, corresponding to a coverage interval of 67 %. Table 8 shows the results of the cell comparison (since the reference cell measured, the working standard cell Al 10/09, had been previously compared against the national standard cell 'Al sealed', the corrections given are relative/traced to the national standard 'Al sealed'). The results of all the methodologies are given in tables 9-13 and summarised in figure 8.

Table 8. Results of the corrections assigned to the five aluminium cells tested after the direct cell comparison.

Cell	*W* (corrected)	Test cell – Al 10/09 mK	Result traceable to National standard cell 'Al sealed' mK	Correction (to 'Al sealed') mK
Al 10/09	3.375 918 350	—	—	3.18
Cell A	3.375 933 950	4.87	1.69	– 1.69
Cell E	3.375 925 376	2.19	– 0.99	0.99
Cell H	3.375 925 358	2.19	– 0.99	0.99
Cell N	3.375 925 435	2.21	– 0.97	0.97
Cell S	3.375 927 960	3.00	– 0.18	0.18

Table 9. Correction obtained for the different methods for supplier A.

Assay	SIE		OME		Hybrid	
Origin	Correction /mK	Uncertainty /mK	Bound /mK	Uncertainty /mK	Correction /mK	Uncertainty /mK
Supplier	-0.13	0.25	0.44	0.26	1.81	0.22
Lab 1	-2.19	1.27	1.09	0.63	-0.65	1.27
Lab 2	-2.43	3.28	1.64	0.94	-1.08	3.24
Lab 3	33.37	35.97	32.92	19.01	0.51	2.54

Upper Limit	Scheil (free *k*)			Scheil (*k* = 0)	
	Correction /mK	Uncertainty /mK	*k*	Correction /mK	Uncertainty /mK
0.25	-3.39	0.27	4.82	-0.50	0.35
0.50	-3.85	0.32	3.72	-0.96	0.21

Gradient Method		Thermal Analysis		Cell comparison	
Correction /mK	Uncertainty /mK	Correction /mK	Uncertainty /mK	Correction /mK	Uncertainty /mK
-0.48	0.27	1.80	0.14	-1.69	0.93

Table 10. Correction obtained for the different methods for supplier E.

Assay	SIE		OME		Hybrid	
Origin	Correction /mK	Uncertainty /mK	Bound /mK	Uncertainty /mK	Correction /mK	Uncertainty /mK
Supplier	0.56	0.57	0.58	0.34	2.17	0.02
Lab 1	0.70	0.21	1.31	0.76	2.10	0.11
Lab 2	0.08	0.79	1.11	0.64	1.52	0.51
Lab 3	3.93	4.29	4.46	2.58	1.60	0.51

Upper Limit	Scheil (free *k*)			Scheil (*k* = 0)	
	Correction /mK	Uncertainty /mK	*k*	Correction /mK	Uncertainty /mK
0.50	17.09	8.91	0.83	1.82	0.19
0.80	6.44	1.76	0.62	1.31	0.11

Gradient Method		Thermal Analysis		Cell comparison	
Correction /mK	Uncertainty /mK	Correction /mK	Uncertainty /mK	Correction /mK	Uncertainty /mK
1.06	0.17	2.10	0.18	0.99	0.93

Table 11. Correction obtained for the different methods for supplier H.

Assay	SIE		OME		Hybrid	
Origin	Correction /mK	Uncertainty /mK	Bound /mK	Uncertainty /mK	Correction /mK	Uncertainty /mK
Supplier	5.62	2.63	6.54	3.78	1.27	0.53
Lab 1	0.20	0.15	0.72	0.42	1.93	0.13
Lab 2	0.08	0.50	0.88	0.51	1.79	0.38
Lab 3	6.08	6.13	6.82	3.94	1.72	0.56

Upper Limit	Scheil (free *k*)			Scheil (*k* = 0)	
	Correction /mK	Uncertainty /mK	*k*	Correction /mK	Uncertainty /mK
0.50	23.66	30.31	0.86	1.77	0.31
0.80	6.80	4.24	0.60	1.24	0.27

Gradient Method		Thermal Analysis		Cell comparison	
Correction /mK	Uncertainty /mK	Correction /mK	Uncertainty /mK	Correction /mK	Uncertainty /mK
0.90	0.18	2.01	0.36	0.99	0.93

Table 12. Correction obtained for the different methods for supplier N.

Assay	SIE		OME		Hybrid	
Origin	Correction /mK	Uncertainty /mK	Bound /mK	Uncertainty /mK	Correction /mK	Uncertainty /mK
Supplier	-0.23	0.45	0.32	0.18	3.15	0.31
Lab 1	0.13	0.10	0.47	0.27	3.35	0.08
Lab 2	-0.26	0.35	0.45	0.26	3.08	0.61
Lab 3	10.33	10.71	9.54	5.51	3.42	0.31

Upper Limit	Scheil (free *k*)			Scheil (*k* = 0)	
	Correction /mK	Uncertainty /mK	*k*	Correction /mK	Uncertainty /mK
0.25	7.29	7.80	0.41	2.85	0.16
0.50	16.35	4.45	0.76	1.39	0.30

Gradient Method		Thermal Analysis		Cell comparison	
Correction /mK	Uncertainty /mK	Correction /mK	Uncertainty /mK	Correction /mK	Uncertainty /mK
1.50	0.20	3.32	0.28	0.97	0.93

Table 13. Correction obtained for the different methods for supplier S.

Assay	SIE		OME		Hybrid	
Origin	Correction /mK	Uncertainty /mK	Bound /mK	Uncertainty /mK	Correction /mK	Uncertainty /mK
Supplier	-0.11	0.31	0.34	0.20	1.90	0.26
Lab 1	0.34	0.23	0.92	0.53	1.93	0.16
Lab 2	-0.04	0.34	0.49	0.28	1.92	0.27
Lab 3	8.13	8.00	8.42	4.86	2.10	0.36

Upper Limit	Scheil (free *k*)			Scheil (*k* = 0)	
	Correction /mK	Uncertainty /mK	*k*	Correction /mK	Uncertainty /mK
0.50	4.56	1.80	0.43	1.97	0.22
0.80	5.94	4.14	0.49	1.49	0.13

Gradient Method		Thermal Analysis		Cell comparison	
Correction /mK	Uncertainty /mK	Correction /mK	Uncertainty /mK	Correction /mK	Uncertainty /mK
1.41	0.33	2.12	0.23	0.18	0.93

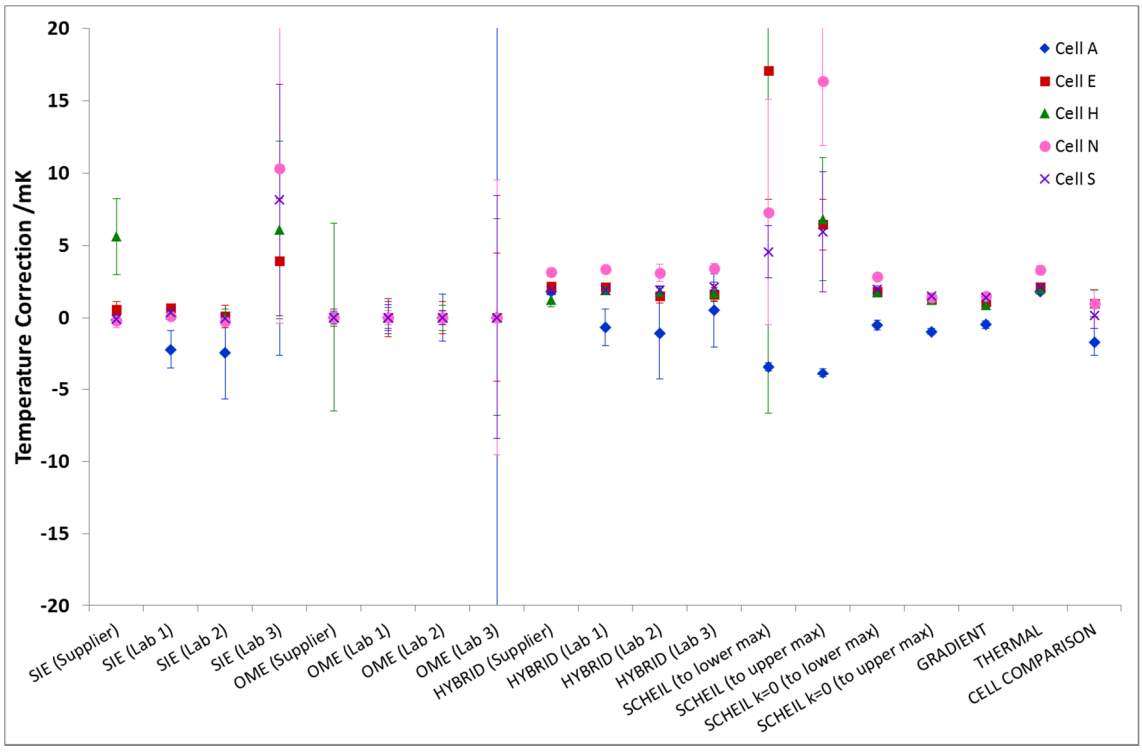

Figure 8. Comparison of the different correction methods, for the five cells.

7. Discussion

Considerable variation in the quality of the chemical analyses was observed. Very little information was given regarding the uncertainty of the measurements. Unless otherwise stated, the uncertainty was assumed to be equal in magnitude to the stated amount of impurity. The uncertainty in the liquidus slopes was obtained from [35].

An example of the irregularities present can be seen in the SIE corrections for the metal from supplier H. The resulting corrections were large, with large uncertainties, because an ICP-AES (inductively coupled plasma atomic emission spectroscopy) analysis was performed, which does not have sufficient sensitivity to detect impurities at the level of parts per billion. The analyses using the supplier's own assay are therefore included for illustration only.

Despite showing poor agreement with each other in general, the GDMS results from Labs 1, 2 and 3 for the metal from Supplier A were very consistent with respect to the titanium (Ti) content of the material. Ti is a significant impurity in Al because it is commonly observed in relatively large concentrations, and because it has a high value of k (about 6.4). However, for Ti the uncertainty declared by Lab 2 is a factor of 10 larger than that of Lab 1. This explains why the SIE and hybrid SIE/OME corrections for Lab 1 and 2 are similar but the uncertainties are quite different. The metal of Supplier A was remarkable because the consistently high levels of Ti indicated by the various GDMS analyses coincided with the observed shape of the freezing curve, which exhibited a large downward slope at the beginning of the freeze, consistent with the shape that would be expected from a high k impurity [25]. This is evident in figure 1.

The GDMS analysis from Lab 3 presented some uncommon peaks of Se (from 13 ppm to 113 ppm) in the metal from all suppliers, which does not correspond to the nominal purity of the samples (maximum nominal impurity content < 1 ppm). Since this was unique to the Lab 3 analysis, it is suspected that some contamination occurred during the execution of the GDMS analysis procedure. The results from Lab 1 for metal E showed an unusually high peak of Bi (1.7 ppm). This lab reported that the sample had been checked with a second GDMS apparatus and the Bi peak proved to be reproducible. However, the liquidus slope of Bi in Al is very small (-0.039 mK/ppm), so the overall contribution from the Bi is just -66 μK, i.e. producing no observable effect on the freezing curve.

The supplier's GDMS results for metal E showed only 0.9 ppm of Si as a detected impurity. No further information was available concerning which elements were analysed, or the detection limits and uncertainties. Since the hybrid SIE/OME method uses GDMS data only for impurity with $k < 0.1$, the SIE component was zero.

Fitting of the Scheil model was performed over selected ranges using a lower limit of $1 - F = 0.05$ and upper limits of both $1 - F = 0.5$ and $1 - F = 0.8$, to give an indication of the sensitivity of the method to the range of the freezing curve over which fitting was performed. However, these limits were not possible for the metals A and N. For these two metals, upper limits of $1 - F = 0.25$ and $1 - F = 0.5$ were employed. Metal A consistently presented a high peak (about 2 mK above the mean temperature of the plateau) at the beginning of the freeze, indicating the presence of a high k impurity, almost certainly Ti, as a high Ti concentration was indicated by all the GDMS analyses. For fitting of the Scheil model with k fixed at zero, this peak at the beginning had to be excluded from the fit.

A key result which is evident in figure 8 is the relatively large variation in the corrections which depend on the GDMS analyses. This is attributable to the very large inconsistencies in the GDMS results from different providers, for the same metal samples. The methods which exhibited the best consistency (i.e. quantitative agreement) were the Hybrid SIE/Modified-OME method, and the Scheil method (provided k was fixed at zero in the fit). Both these methods are insensitive to errors in the GDMS analysis. This is because the SIE component of the hybrid SIE/Modified-OME method only takes into account impurities with $k > 0.1$, so that relatively large amounts of impurity are needed to effect a given temperature depression compared with impurities having $k < 0.1$, while the Scheil method does not rely on the GDMS analysis at all.

Conclusions

For the first time, a suite of five aluminium fixed point cells, each constructed using aluminium from a different source, has been subjected to a systematic analysis of impurity correction methods by obtaining a series of freezing curves measured under identical conditions for all five cells. Also for the

first time, GDMS analyses were obtained from three different providers for each of the five metals used. By placing the investigation on a systematic basis in this way, it was possible to draw some general conclusions about the accuracy of the different impurity correction methods, and the accuracy of the GDMS assays. The methods evaluated were the SIE, OME, Hybrid SIE/Modified-OME, Scheil fitting, gradient method, thermal method, and direct cell comparisons (the OME itself is not considered a correction methodology but the estimate of a bound, which is applied as the uncertainty of the cell due to impurities). In general, the GDMS assays exhibited large discrepancies in comparison to each other, making it difficult to rely on correction methods (or estimated bound in the case of OME) that are solely dependent on them. It was shown that the recommended CCT approaches of SIE and OME gave the most inconsistent results. This is because it appears impossible to get the reliable GDMS data on which both approaches rely. The most consistent correction methods were the hybrid SIE/Modified-OME method, and the Scheil method with the distribution coefficient k fixed at zero. The former only depends weakly on the GDMS analysis, while the latter relies only on the shape of the freezing curve. It is recommended that these two approaches, in favour of the SIE/OME approaches, are used in combination to determine reliable impurity corrections, with robust uncertainties, for ITS-90 fixed point temperatures.

Acknowledgments

This work was funded by the EURAMET European Metrology Research Programme (EMRP) project 'Novel Techniques for Traceable Temperature Dissemination (NOTED)'. Rodrigo da Silva would like to acknowledge the Brazilian scholarship programme Science Without Borders. The authors thank Jayne Gray and Radka Veltcheva of NPL for their valuable contributions to the experimental arrangements. Eric Bennett, Madeleine Peck, and Steve Spencer of NPL are gratefully acknowledged for their help with the auxiliary chemical analyses, and Sumitomo Corporation of Japan for kindly donating some sample material.

References

[1] H. Preston-Thomas 1990 The International Temperature Scale of 1990 (ITS-90) *Metrologia* **27** 3-10 and 107

[2] Mangum B W *et al* 1999 On the influence of impurities on fixed-point temperatures *Working Document* CCT-WG1 CCT/99-11

[3] Standard guide for use of freezing-point cells for reference temperatures (2003) *ASTM Standards* document E 1502-98

[4] Fellmuth B and Hill K D 2006 Estimating the influence of impurities on the freezing point of tin *Metrologia* **43** 71

[5] Yamazawa K, Widiatmo J V and Arai M 2007 Thermal analysis of the heater-induced realization of the tin fixed point *Int. J. Thermophys.* **28** 1941

[6] Widiatmo J V *et al* 2011 Study on the realization of zinc point and the zinc-point cell comparison *Int. J. Thermophys.* **32** 309

[7] Sun J *et al* 2014 Effect of ultra-trace impurities on the freezing point of zinc *Int. J. Thermophys.* **35** 1134

[8] Krapf G *et al* 2012 Influence of impurities on the fixed-point temperature of zinc: estimations by the SIE method and practical limitations *Meas. Sci. Technol.* **23** 074022

[9] Žužek V *el at* 2014 Open zinc freezing-point cell assembly and evaluation *Int. J. Thermophys.* **35** 1147

[10] Widiatmo J V *et al* 2006 Estimation of impurity effect in aluminium fixed-point cells based on thermal analysis *Metrologia* **43** 561

[11] Widiatmo J V *et al* 2008 Impurity effect in silver-point realization *Int. J. Thermophys.* **29** 158

[12] Widiatmo J V *et al* 2011 Confirming impurity effect in silver-point realization from cell-to-cell comparisons *Int. J. Thermophys.* **32** 2281

[13] Fahr M and Rudstch S 2008 A new method for the quantification and correction of thermal effects on the realization of fixed points *Int. J. Thermophys.* **29** 126

[14] Rudtsch S *et al* 2008 High-purity fixed points of the ITS-90 with traceable analysis of impurity contents *Int. J. Thermophys.* **29** 139

[15] Fahr M and Rudtsch S 2009 Oxides in metal fixed points of the ITS-90 *Metrologia* **46** 423
[16] Fahr M, Rudtsch S and Aulich A 2011 Further findings of impurity precipitation in metal fixed points *Int. J. Thermophys.* **32** 2239
[17] Fellmuth B *et al* 2005 Methodologies for the estimation of uncertainties and the correction of fixed-point temperature attributable to the influence of chemical impurities *Working Document* CCT-WG1 CCT/05-08
[18] Pearce J 2014 Distribution coefficients of impurities in metals *Int. J. Thermophys.* **35** 628
[19] Hill K D and Rudtsch S 2005 Thermometry's dependence on chemical metrology: a needs-based assessment *Metrologia* **42** L1
[20] Ripple D *et al* 2003 Report presented to the CCT by Working Group 1 *Working Document* CCT-WG1 CCT/03-23
[21] Moiseeva N P 2003 The role of the impurity component in the budgets of uncertainties, *Working Document* CCT-WG1 CCT/03-24
[22] Yamazawa K *et al* 2008 Limits of the SIE and the thermal analysis on impurity effect evaluation *Working Document* CCT-WG1 CCT/08-03
[23] Widiatmo J V, Harada K and Arai M 2004 Analyzing metal fixed-point cells from their plateaus *Proc. SICE Annual Conf.* 1936
[24] Head D I *et al* 2008 The comparison of MTDATA with the melting/freezing point curves of ITS-90 metal fixed points *Int. J. Thermophys.* **29** 1796
[25] Pearce J V, Veltcheva R I and Large M J 2013 Impurity and thermal modelling of SPRT fixed-points *Temperature: Its Measurement and Control in Science and Industry* vol. 8, Proc. AIP Conf., **1552** 283
[26] Malik Z *et al* 2011 A solidification approach to correcting for the effect of impurities in fixed points *Int. J. Thermophys.* **32** 1589
[27] Pearce J V *et al* 2012 Optimization of SPRT measurements of freezing in a zinc fixed-point cell *Metrologia* **49** 359
[28] Widiatmo J V 2004 A survey on the uncertainty in the realization of ITS-90 metal fixed points due to impurities *AIST Bulletin of Metrology* vol. 3 **2** 318
[29] Renaot E, Valin M H and Elgourdou M 2008 Influence of impurities and filling protocol on the aluminium fixed point *Int. J. Thermophys.* **29** 852
[30] Ancsin J 2003 Impurity dependence of the aluminium point *Metrologia* **40** 36
[31] Renaot E 2008 Evidence of furnace-related aluminium cell contamination *Acta Metrologica Sinica* **29**
[32] Renaot E and Martin C 2011 Aluminium fixed point: impact of the time spent in the liquid phase on the liquid-solid transition and obviousness of the pollution of the ingot *Int. J. Thermophys.* **32** 1496
[33] Head D I, Petchpong P and Au J Y H 2008 Effects of impurities on the melting curve of the aluminium fixed point *Acta Metrologica Sinica* **29**
[34] Petchpong P and Head D I 2011 The influence of titanium on the aluminium fixed-point temperature *Int. J. Thermophys.* **32** 1507
[35] Pearce J V, Gisby J A and Steur P P M 2016 Liquidus Slopes for Impurities in ITS-90 Fixed Points, *Metrologia*, accepted
[36] Guide to the Realization of the ITS-90: Metal Fixed Points for Contact Thermometry (http://www.bipm.org/en/committees/cc/cct/guide-its90.html)
[37] Mangum B W *et al* 2002 Summary of comparison of realizations of the ITS-90 over the range 83.8058 K to 933.473 K: CCT Key Comparison CCT-K3 *Metrologia* **39** 179
[38] Heyer D *et al* 2008 Final report on EUROMET T-K4 (EUROMET Project 820): Comparison of the realizations of the ITS-90 at the freezing points of Al (660.323 °C) and Ag (961.78 °C) *Metrologia* **45** Tech. Suppl. 03003
[39] Guide to the Realization of the ITS-90: Platinum Resistance Thermometry (http://www.bipm.org/en/committees/cc/cct/guide-its90.html) to be published
[40] Pearce J V *et al* 2013 Self-validating Type C thermocouples using high temperature fixed points *Temperature: Its Measurement and Control in Science and Industry* vol. 8, Proc. AIP Conf. **1552** 595

[41] Rudtsch S 2011 Procedure for the impurity-related correction at the indium fixed-point *Int. J. Thermophys.* **32** 293
[42] Ripple D *et al* 2008 Recommended list of common impurities for metallic fixed-point materials of the ITS-90 *Working Document* CCT/08-16
[43] White D R *et al* 2009 Uncertainties in the Realisation of the SPRT Subranges of the ITS-90 *Working Document* CCT/08-19/rev (http://www.bipm.org/cc/CCT/Allowed/24/D19_rev_WG3_Doc_rev_10July2009.pdf)
[44] Rudtsch S 2005 Cryoscopic constant, heat and enthalpy of fusion of metals and water *Working Document* CCT/05-04/rev